https://doi.org/10.1016/j.nanoen.2018.11.086

Nanophotonic energy storage in upconversion nanoparticles

Mingzi Sun[1#], Hao Dong[2#], Alan William Dougherty[4], Qiuyang Lu[1], Wing-Tak Wong[1], Bolong Huang[1]*, Dengfeng Peng[5], Ling-Dong Sun[2], Chun-Hua Yan[2,3]*

1. *Department of Applied Biology and Chemical Technology, The Hong Kong Polytechnic University, Hong Hum, Kowloon, Hong Kong SAR, China.*
2. *Beijing National Laboratory for Molecular Sciences, State Key Laboratory of Rare Earth Materials Chemistry and Applications, PKU-HKU Joint Laboratory in Rare Earth Materials and Bioinorganic Chemistry, College of Chemistry and Molecular Engineering, Peking University, Beijing 100871, China.*
3. *College of Chemistry and Chemical Engineering, Lanzhou University, Lanzhou 730000, China.*
4. *Department of Computing, The Hong Kong Polytechnic University, Hong Hum, Kowloon, Hong Kong SAR, China.*
5. *Key Laboratory of Optoelectronic Devices and Systems of Ministry of Education and Guangdong Province, College of Optoelectronic Engineering, Shenzhen University, Shenzhen 518060, China.*

*Email: bhuang@polyu.edu.hk (BH); yan@pku.edu.cn (CHY)

#: These authors contribute equally.

Abstract

In nanophotonic energy storage, an energy conversion model is established for intrinsic nanophotonic energy storage (NPES) effects. Here we realize that the charge inhomogeneous distribution on the surface of upconversion nanoparticles (UCNPs) would persistently exist as well as the formation and migration of surface defects states despite of the compound component ratio, even following the stringent stoichiometric ratio. Our preliminary efforts on NPES effect has recognized from the recent published work [***Nature*** 561, 88 (2018)], which the surface quantum confinement arose because of a recently found surface vacancy induced Coulomb states (SVIC) states. Further in-depth excavation on surface charge density distributions and defect orbitals of surface localized electronics and holes have affirmatively repeated the Guerra's theory [***Nature*** 554, 346 (2018)] and reflected the existence of surface defect states in both stoichiometric and non-stoichiometric compounds. Therefore, beyond the experimental trail-based multi-doping chemical modifications, we proposed the surface electronic process for efficient NPES effect can be modulated by an intrinsic level-matching induced surface resonant quantum tunneling (LM-SRQT) in this work. The UCNP size-effect can be confirmed that simply might be not an influencing factor of dominating NPES effect while the surface degree of non-crystallizations indeed matters.

Introduction

Nowadays in the realm of nanoenergy[1-3], nanophotonic storage underlies an interplay from two different sets of photo-electronic transitions with the entanglement of time-and-spatial energy conversions, which is facing an unprecedented challenge jumping beyond the conventional mazing patterns of experimental attempts and demands theoretical mechanistic guiding studies than ever before. Increasing needs with stronger intensity, longer lifetime, lower cost and broader spectrum for quantum dot scintillation (X-ray luminescence)[4], bio-in-vivo imaging (fluorescence), illuminating materials engineering (phosphorescence)[5], etc. are rapidly expanding. It presents greener and more efficient features than conventional luminescence device that can store the excitation energy and slowly release by a photonic emission lasting for several hours [6-7]. The most promising application is in the blockage, storage and secondary conversion of hazard high energy X- or γ-rays (scintillation imaging) or in-vivo bioimaging without external excitation needed on living-tissues [8-9]. In addition, the theoretical study of the underlying mechanism will be also beneficial to the in-depth insight of other energy transfer and storage process of novel energy devices [10-12].

Nanophotonic energy storage (NPES) materials are endowed with a typical class of slow-release (ultra-long-lived) trapped charge carriers towards recombination after cessation of external excitation energy [13-16]. It could accept a broad spectrum scaling from X-ray to near-infrared (NIR). However, it is critical that the NPES applications are still constrained by enormous difficulties in realizing a universal modulation from convention experimental synthesis protocols. Current consensus reaches on two dominant factors of determining the NPES performance: activators and trapping-centers. The activators are photonic output emission centers with electron-hole recombination after being excited. Such emission wavelength is mainly determined by the intraconfigurational levels as intermediate for electrons and holes transport given by activators. Transiently excited energies are accordingly stored *via* localizing the excited electrons at the trapping-centers after absorbed externally irradiated photons. Energy can be further released by thermal or photostimulations *via* charge recombination from the gradually released localized electrons or holes towards the emitters. The output intensity and duration time of NPES effect are governed by the concentrations and depths of trap centers. In detail, the direct recombination process of luminescence centers with released electrons from shallow traps governs the intensity. Indirect recombination usually produces weak but long-lasting luminescence by a slow tunneling rate, which dominates the life-time extension. Electrons at deep-traps with long-lifetime can also be ionized from nearby dopants based on a reversible tunneling effect. Therefore, in the design of a tailor-made the NPES material, a suitable activator of demanded emission wavelength and a proper host capable of creating appropriate trap centers to storage excitation energy in the way of localizing electrons under proper levels, so as to actualize NPES are required [17-19].

Persistent luminescence is a typical example of the NPES effect. Related materials and devices with NPES effect have been rapidly developed in the past decade [20]. Among them, $CaAl_2O_4:Eu^{2+}$, Nd^{3+} and $SrAl_2O_4:Eu^{2+}$, Dy^{3+} have been well commercialized and widely used in various relevant fields [21], especially in medical diagnostics. They provide sufficiently strong and long-lasting (>19 hrs) persistent luminescence that able to be excited by sunlight and room light [5, 16].

In general, to modulate the persistent luminescence properties flexibly in the whole wavelength, chemical doping is an effective strategy to modify the electronic structure and surface property of luminescence materials such that their performance can be significantly

improved [17, 22]. In combination with specific conditions of synthesis, the appropriate trap levels in the materials have been attempted out for controlling the required NPES related luminescence properties [17-19, 22-25]. Nevertheless, the exact theoretical mechanism is still not clarified.

To address this fundamental challenge, a universal *inversed-design* from energy-transfer model with corresponding experimental synthesis route has been proposed to realize the NPES concept in general luminescence nanomaterials (**Figure 1a**). Implicit energy paths based on intrinsic charge-complemented surface defects can be collaborated to downscale the extremely wide bandgap and benefit the charge-separation for recombination-extension (**Figure 1b**). The LM-SRQT effect plays as a determining driving force to accomplish the subsequent de-excitations of excited charge carriers for recombination after the spatial charge separations induced by harvested energy conversion. The surface electronic confinement is expected to be a general prerequisite for NPES relying on surface defects induced by non-crystallization for luminescence modulation (**Figure 1c**). Synthesis routes are capable of not only modifying the morphology of the NPs but also modulating the overall electronic behaviors [26-31], which can be distinguished from the general oleic-capping effect.

Recently, Guerra *et al.* have clearly unveiled the surface defect behaviors on general nanoparticles [32], especially the defect evolutions on spherical NPs. Inheriting this pioneering work, here we realize that charge inhomogeneous distribution on the surface of any nanoparticles could be always observed as well as the formation of the mobile surface defect states regardless compound percentages, even following the stringent stoichiometric ratio. We also realized the NPES effect in our recently published work [4]. The newly discovered Coulomb states caused by the surface vacancy defects can contribute to the surface quantum confinement [4]. Here in this work, our further disinterment on surface charge density distributions and defect orbitals of surface localized electronics and holes have affirmatively repeated the Guerra's theory [32] and confirmed the formation of surface defect states with both stoichiometric and non-stoichiometric. Therefore, in the present study, we proposed the surface electronic process for efficient NPES effect can be modulated by the LM-SRQT. As supported by recent works [4, 32], even the system following with stoichiometric ratio still forms the surface defects. We confirm that the NP size-effect is simply not an influencing factor of dominating NPES effect while the surface degree of non-crystallizations indeed matters.

Theoretical and Experimental Methods

DFT calculations. To determine the electronic properties at the ground states, density functional theory (DFT) calculations are performed. We use the CASTEP (Cambridge Serial Total Energy Package) source code to perform calculations with the DFT+U method [33]. A hexagonal lattice with the $P\bar{6}$ space group is modeled for β-phase $NaREF_4$ (Ln=Y, Gd, and Lu). The norm-conserving pseudopotentials for Na, Y, Gd, Tb, Er, Tm, Lu and F atoms are generated using the OPIUM code in the Kleinman-Bylander projector form [34], and the non-linear partial core correction [35] and a scalar relativistic averaging scheme [36] are used to treat the spin-orbital coupling effect. In particular, we treated the (4f, 5s, 5p, 5d, 6s) states as valence states of the Gd, Tb, Er, Tm, and Lu atoms, respectively. The RRKJ method is chosen to optimize the pseudopotentials [37].

For all the electronic state calculations for $NaREF_4$ (RE=Y, Gd, and Lu), we use the self-consistent determination for the U correction on the localized 4f orbitals to correct the on-site Coulomb energy of the electron spurious self-energy. In previous studies, we established a

manner to determine the on-site electronic self-energy and related wave function relaxation in the semicore d or f orbitals in heavy elements with mixed valences to obtain accurate orbital eigenvalues for the electronic structures and transition levels [38-44]. An ab initio two-way crossover searching calculation is performed using two different functionally compiled CASTEP-17 developing source codes [42, 45-46]. This process was described in detail in our previous works. With our self-consistent determination process, the on-site Hubbard U parameters for 4f of Er and Tm and different 2p of F-sites are obtained. The time-dependent density functional theory (TD-DFT) calculation is then performed with the two-electron-based Tamm-Dancoff approximation[47] imported from our self-consistent corrected ground-state wave function, which is crucial for two-photon absorption (TPA) calculations.

To elaborate the excited states, the related calculations for β-$NaREF_4$ doped with different trivalent lanthanide ions (Ln^{3+}, from La to Lu) are examined with a series of TD-DFT calculations. These excitation energies correspond to the locations of absorption peaks in the optical spectrum of a material and are more accurate than Kohn-Sham excitation energies. Some of the de-excitation paths between different energy levels correspond to the emission peaks from the output luminescence spectrum. The calculations are performed using the Tamm-Dancoff approximation [47]. This method enables us to calculate the full set of optical properties with the support of the excitation energies and corresponding transition probabilities. This study is also applicable to low-dimensional $NaREF_4$ systems since additional effects such as boundary, quantum-confinement, and different coordination-induced mixed-valence effects can be considered.

Preparation of $Y(CF_3COO)_3$ precursors. A given amount of Y_2O_3 (China Rare Earth Online Co., Ltd., > 90%) was added to a flask containing excess amount of trifluoroacetic acid (Sigma-Aldrich., >80%). The slurry was heated under stirring till a clear solution formed. $Y(CF_3COO)_3$ precursors were obtained after filtering, concentrating and drying.

Synthesis of oleate modified $NaYF_4$ nanoparticles. $NaYF_4$ nanoparticles were synthesized in oleic acid (OA) and oleylamine (OM) with a thermal decomposition method [48]. 1 mmol CF_3COONa and 1 mmol $Y(CF_3COO)_3$ precursors were added to a three-necked flask containing OM and OA (20 mL, volume ratio 9:1) at room temperature. The slurry was heated to 110 °C for removing water and oxygen under vigorous stirring. Then, a clear solution formed and was heated to 280 °C for reaction (15 min) under N_2 atmosphere. After cooling to room temperature, an excess amount of ethanol was added to precipitate the nanoparticles. The nanoparticles were collected by centrifugation at 7800 rpm/min for 10 min. Finally, the nanoparticles were redispersed in 10 mL cyclohexane.

Preparation of OA-free $NaYF_4$ nanoparticles. A facile ligand-exchange was used to synthesis high quality OA-free nanoparticles [49]. 1 mL colloidal solution containing oleate-$NaYF_4$ nanoparticles were dispersed in a mixture containing 5 mL cyclohexane and 5 mL DMF. Then, 30 mg $NOBF_4$ was added. The slurry was stirred for 30 min at room temperature to leave oleate ligands in cyclohexane, while the naked nanoparticles transfer to DMF phase. The DMF phase was removed for centrifugation by adding an excess amount of toluene (18000 rpm/min, 15 min). The OA-free nanoparticles were redispersed in DMF for further characterizations.

Characterization of $NaYF_4$. Samples for TEM and HRTEM examination were prepared by drying a drop of colloidal solution dispersed with $NaYF_4$ nanoparticles onto a copper grid. TEM and HRTEM measurements were performed with a JEOL JEM-2100F TEM operated at

200 kV. XRD patterns were recorded on the Bruker D2 PHASER diffractometer (Germany), using Cu Kα radiation (λ = 1.5406 Å). Fluorescence excitation and emission spectra were recorded on a Hitachi F-4500 spectrometer, while the decay curve of $NaYF_4$ colloidal solution was examined on a FLS980 steady state and time-resolved fluorescence spectrometer (Edinburgh Instruments). Decay curves at varied temperature were monitored on a Deltaflex UltraFast lifetime Spectrofluorometer (Horiba Jobinyvon IBH Inc.). Excitation source for the decay curve measurements was a 340 nm pulsed laser.

Results and Discussion

NPES electronic investigation and surface resonant quantum tunneling effects. The RE based fluoride system has gradually become the optimal system for demonstrating our mechanistic study on the NPES effect. Representative compounds like $NaREF_4$ (RE=Y, Gd, and Lu) have substantially low phonon-electron scattering and coupling rate guaranteeing photon-induced electronic transitions can be carried out at a higher efficiency [48, 50]. Moreover, these systems present very low photo-induced charge carrier combination rate within the bulk region at large sizes providing a good prerequisite host-system for the extended life-time manipulations via engineering of nanosize surface electronic process modulations. As downscaling to nanoparticles (NPs), the surface effect turns to even stronger and more sensitive than other ordinary electronic nano- or bulk-materials, owing to their much more evident quenching effect arising from their 5d/4f orbital based excited states response under external irradiation, even as low as near-infrared pulse laser energies [29]. Therefore, these preconditions for non-doped native $NaREF_4$ NPs pave an avenue for our exploration on their entangled fast-low electronic process as a cornerstone of the NPES effect.

Inspired from the surface defect behaviors of nanoparticles from the work of Guerra *et al.* [32], the charge inhomogeneous distribution on the surface have also been considered in our work. The induced formation and migration of surface defects states would exist even in the compound following the ideal stoichiometric ratio. Our recent work on inorganic oscillator supported this conclusion since SVIC can largely confine the exciton behaviors and the luminescence performance [4]. From the structural view, it can be understood as the surface sites are directly truncated from the infinite bulk lattice with periodic expansion. Our further calculations of surface charge density distributions and surface defect orbitals have affirmatively reproduced the results of Guerra's theory [32] and confirmed the surface defect states in both stoichiometric and non-stoichiometric ratios (**Figure 2**). In details, we find that the surface charge density distributions and orbitals of differently sized $NaYF_4$ NPs clearly and objectively reflect the non-crystalized area on the surface lattice after the relaxation of the under-coordinated cationic Na-, Y- and anion F-sites.

On illustrations of surface active orbital densities distributions, the three-dimensional (3D) real-spatial contour plots of the related electronic density fields have been generated (**Figure 2a-c**) corresponding to exact each atomic site within the host lattice. This indeed represents the real place where the inter-ionic valence orbital can be active for responsible for overall external excitations. In another word, we confirm that surface alkaline ions like Li, Na, and K sites are playing a central role for stabilizing surface and in-bulk photo-generated local micro-electric-fields, but evidently inert to the external photo-excitations

The surface modification method is the key tool that usually apply to passivate the surface defects, which have been usually considered that cannot contribute to the efficient energy transfer of nanoparticles. To accurately locate the spatial distributions for transient energy

storage sites, we further visualize the localized electronic and hole trapping orbitals from the surface defect states, where have been accurately calculated from the electronic structures and the optical fundamental band gap of these three different-sized $NaYF_4$ NPs models (**Figure 2d-f**). We clearly see that only the surface states produce the localized electronic (occupied) and hole (unoccupied) states within the optical band gap, which shows agreement and consistency with our previous experimental deduction that with and without the core@shell protection [41, 51]. This further indicates that the in-bulk lattice of the NPs is "*photo-electronically transparent*" region. Especially regarding the coverage of inert shell layer, these localized electronic and hole orbitals on the surface are the quenching states that are responsible to either storage or deplete the energy transfer within the host matrix at the in-core area [52]. In addition, Na-sites on the surface of the $NaYF_4$ particle models are electronically inactive since there are no charges distributed around the Na-sites. Thus, we confirm that the surface inhomogeneous electronic states of the NPES NPs are predominantly attributed to the under-coordinated or defective F- and Y-sites or other tri-positively charged lanthanide ion sites. For the contribution of the alkaline cation such as Na^+ or Li^+ in $NaLnF_4$ (Ln=lanthanides), they contribute more to stabilizing the local electrical field of the host matrix.

To exclude the size effect on the surface electronics, here we further examine such evolution that induces the physicochemical trend for the surface energy variation (**Figure 2g**). Such size-effect investigation involves these three NP models to clearly illustrate the subtle interplay among the surface energy, surface area, and the surface-to-volume ratio. We scale the size regarding the number of atoms, namely, 48, 201, and 418 atoms, respectively. However, this has strongly deviated from $\propto R^2$ or $\propto R^3$ (R: NP radius), meaning what we find is the surface area scales approximately linearly with the total number of atoms for the NPs. This implies the surface electronic active defect sites or optically inhomogeneous area very possibly un-follows the area or bulk distribution. Therefore, during the growth process, "regulating the integrity of the NPs" is an important driving force as the number of atoms increases and shaping will be more constrained for synthesizing NPES NPs.

Next, we evaluate the variation in the surface energy area density σ_s, which is another vital energetic indicator. The changing behavior of σ_s will be transformed into the driving force of the final equilibrium stage of the NPs. We show that the area density σ_s nearly converges in the form of exponential decay to a given value, approaching -0.97 eV/Å^2 (**Figure 2g**). This decay indicates that with the increasing size of the UCNPs, the surface energy area density σ_s will converge to a constant value, which involves a transition from the quantum confinement effect to the bulk effect with increasing size. Meanwhile, the surface-to-volume ratio is another significant indicator that can also distinguish between the quantum confinement and the bulk effects, since it also exponentially decays to converge to 0.27 Å^{-1}. Notably, this converged surface-to-volume ratio is nearly 5.5 times lower than the Thomas-Fermi screening length constant (i.e., 1.38 Å^{-1} for the free-electron gas limit), according to our previous theoretical methodology discussion [42]. This difference implies that for larger UCNPs, the electrons are still strongly localized on the surface and within the host matrix of UCNPs. Such electronic transitions are highly capable of non-radiative resonant transfer to sustain the inter-level transitions.

The electronic total density of states (TDOS) of the UCNPs is preliminarily studied based on the ground-state relaxed $NaYF_4$ with different total numbers of atoms (**Figure S1**). With the increasing size, the TDOS becomes smoother with increasingly fewer van-Hove singularities due to the absence of long-range order on the surface. This lack of order arises because the

non-crystallization degree is rather high on the surface of the UCNPs due to the hidden driving force or the regulated shape, with the surface-to-volume ratio and surface energy area density simultaneously converging at the same point (**Figure 2g**). Meanwhile, we find that for the small (48 atoms) $NaYF_4$-based UCNPs following a 1:1:4 stoichiometric ratio, a deep electron state is localized near the middle of the optical band gap (E_V+4.98 eV). Moreover, for larger UCNPs not following the stoichiometric ratio, a quencher level is always present at approximately E_V+3.0 eV above the valence band maximum (VBM), which is one-third the size of the band gap, independently of the total number of atoms. We attribute this localized electronic level to a generalized surface non-stoichiometric ratio effect since the level position is not influenced by the variation in the total number of atoms or different stoichiometric ratios.

Thermodynamically, a high surface-to-volume ratio minimizes the surface energy. Alongside the energy transfer, we studied the thermo-stability limits in these native non-doped NPES hosts (*see* **Table S1-S3** and **Figure S2)**. Native defect formation energy implies two typical vacancies (V_F and V_{Na}) are the dominant influence on the energy levels and related inter-level transitions of UC luminescence. Thermodynamic transition levels (TTLs) reflect the donor trap levels stay at higher positions in the optical fundamental band gap of NPES NPs than the acceptor trap levels. This trend ensures a substantially higher rate of recombination to produce the energy output within the NPs. This energetic scale can also fulfill the non-radiative resonant energy transfer for longer-distance migration from the defect sites to the different rare-earth ion dopant (RE^{3+}) activators. Detailed thermodynamic calculations (**Figure S3)** also show consistency with reported experimental data that illustrated the current synthesis routes have already easily introduced the native point defects such as V_F in either α- or β- phases of $NaREF_4$ systems [53].

For a guaranteed NPES effect, level-matching induced surface resonant quantum tunneling (LM-SRQT) process is the stringent electronic preconditions for screening candidate NPs. To probe more electronic details, single-particle levels (SPL) of the native point defect V_F and V_{RE} have been investigated with Er_Y^{3+} doping (**Figure S4)**. The energy transfer paths via the ionized V_F defect level have been confirmed within these three UCNPs materials. The electronic states of Tb_{Gd}^{3+} doped β-$NaGdF_4$ have also been investigated for characterizing their energy transfer path (**Figure S5)**. We find the highest excitation energy level matches the SPL denoting an absorption enhancement by localized electronic levels. The level-matching is particularly evident in the regions near the CB and VB (**Figure 2h**). It also creates the opportunity for recalling the literature energy transfer theory [5, 30, 54]. Therefore, the quantum tunneling effect for excited electrons within the bulk lattice of the UCNPs can bridge the energy conversion among the same type of defect sites but with *transient* time-scaled excitations and *long-lifetime* localizations. This simultaneous process creates the possibility of extending the emission time decay for the intrinsic NPES.

To descent, we look at the hybrid-path between long life-time electron localization and the transient-state energy transfer by a multi-photon process. Investigated by our *ab-initio* calculated excitation levels and oscillation strength (**Figure S6**), the electrons are excited from the bulk VB to final state trapped at the surface *color-center* via a middle transient and the delocalized CB edge. This means that the energy transfer for long-lifetime luminescence such as that of can be achieved with the assistance of a short-lifetime transient state at-least by pulsed laser excitation or UV excitations. Therefore, it is confirmed size effect is merely not an influencing factor which can be excluded. The NPES behavior turns out to be dominated by the surface degree of non-crystallizations.

Current Synthesis Challenge for the NPES. According to the aforementioned photo-electronic mechanism for NPES, we realize that optimal surface non-crystallization degree with higher surface charge trapping rates are the determining factor to achieve highly efficient surface resonant tunneling effect (LM-SRQT) with extra-long lasting release and recombination for surface electron-hole pairs. However, the current synthesis strategy of the $NaREF_4$ UCNPs has largely suppressed such intrinsic NPES effect [55]. Previous literatures reported the required organic phase environments for synthesis are easy to quench all possible energy transfer routes [29, 56]. In addition, the broad emission of the OA-capped NPs in the visible wavelength range usually exhibits distinct peaks or different profiles when the OA ligands are removed. Even the UV absorption from the NPES NPs still displays similar behavior, which arises from charge-transfer by the OA ligands chemisorption. This further perturbs the surface electronics. Similar fluorescence was detected from the reaction solvent after the nanoparticles were extracted, as introduced in the work of Wang *et al.* [56]. Hence, to address these difficulties brought by capping effect from surface organic ligands, we explore the actual influence of the most common oleate acid (OA)-phase-based synthesis route on the further energy transfers.

Here we briefly consider five different cases of the OA molecules chemically adsorbed on the surface of the $NaYF_4$ (**Figure 3a**). These cases are (1) OA adsorbed at the Na-site on the surface, (2) OA adsorbed at the Y-site on the surface, (3) two F-sites bonded with the C=C double bonds of the OA molecule, (4) Na-site bonded with the C=C double bonds of the OA molecule, and (5) the same adsorption as case (4) but with the direction of the OA molecule reversed. Formation energies (**Table S3**) confirm OA energetically favorable to adsorb onto Y-or RE-site (case 2) of $NaREF_4$, while the alkaline-site adsorption is the second lowest profile. In contrast with the un-capped NPs, the localized HOMO charges have been transferred from the surface of the UCNPs to the different sites of the adsorbed OA molecule (**Figure 3b**). Meanwhile, the surface electronic orbitals of OA-capped molecules also demonstrate newer charge trapping centers transferred from NPs to the adsorbed OA ligand. The electronic trapping centers migration to OA will facilitate the OA-photonic-absorption as broad-band-like energetic depletion, which can be supported by the newer trapping levels induced by the OA-ligand localizing over a wide range within the band gap from near the valence band maximum (VBM) to the midgap (**Figure 3c**). Such trapping levels intensify the energy mismatch between the SPLs and the transient excitation levels of the NPES systems and lead to the impediment of the LM-SRQT process (**Figure 2g**). Therefore, our calculation results can confirm the capped OAs as the depletion centers that produce the mismatched surface electronic localized levels to perturb the realization the NPES. The surface electronic confinement is a generalized mechanism that is concurrent with the growth process of the NPs [31]. Synthesis routes are capable of not only modifying the morphology of the NPs but also modulating the overall electronic behaviors, as previously reported [26-30]. With this finding, we believe that revising the current synthesis routes can possibly highlight an optimal tailoring RE-based NP system from ordinary upconversion to intrinsic NPES effect. Hence, by eliminating the perturb from the OA ligand, the surface quencher electronic states indeed prolong the energy transfer routes through the energy matched quantum tunneling effect (**Figure 3d**).

Mechanism of the prolonged NPES effect. To simply verify the unclarified impact on lowering and extending the NPES effect by current synthesis challenge, the actual decay behaviors of NPES has been studied by experiments. $NaYF_4$ NPs were synthesized through a previously reported thermal decomposition route [55] and monodispersed with polyhedron

morphology and narrow size distribution of 7.6 ± 0.7 nm (**Figure 4a**) following High-resolution transmission electron microscopy (HRTEM) image (**Figure 4b**) and corresponded Fast Fourier Transformation (FFT) pattern (**Figure 4c**) indicate the cubic structure of the nanoparticles. The powder X-ray diffraction pattern (**Figure S7**) also confirmed the structure and composition. The removal of the surface ligands has been conducted by facile ligand exchange method and dispersed in DMF (**Figure 4d**). The steady-state and transient-state fluorescence properties of OA-free NPs were then recorded. As shown in **Figure 4e**, broadband excitation and emission spectra can be noticed, which should be related to the transitions between the energy states of intrinsic vacancies in $NaYF_4$ NPs. As the decay trends shown in **Figure 4f**, two characteristic decay wavelengths have been observed, namely 385 nm and 405 nm., which display similar bi-exponential trend with different decay time. The faster decay was around 1.3 ns (13%, 385 nm)/1.5 ns (18%, 405 nm), while the longer decay approached to 15.9 ns (87%, 385 nm)/14.2 ns (82%, 405 nm). The decay behavior of 405 nm emission was further monitored at the varied temperature from 300 K to 78 K with $NaYF_4$ powders as **Figure 4g**. The preservation of bi-exponential decay trend with progressive extension in emission lifetime from 3.4 ns to 5.0 ns (average lifetime) can be noted (**Table S4**). This should be due to the suppressed lattice vibration (phonon energy) as the temperature decreased, which facilitated the slower depopulation of electrons at excited states. The enhancement for the emission lifetime of $NaYF_4$ in DMF colloidal solution (OA-free nanoparticles) than powder state can demonstrate that the surrounding ligands should be important for perturbing the photonic decay behaviors of the excited vacancies in $NaYF_4$, which is in good agreement with our computational results.

To self-consistently verify the tunneling migration between transient and long-life localized electronic state for prolonging the NPES, satisfying the pure mathematical dynamic modelling can reveal the nature of energy transfer behaviors, which only relies on the occupation of different energy levels. Every differential dynamic equation indicates the various contributions from each region (e.g., internal-bulk of the host and surface) as detailed mathematical expression shown in ***Supplementary Information***. The electronic dynamics for the excitation, cross-sectional relaxation, and emissions have been taken into the mathematical simulation. In the five-energy level modelling, the surface quencher sites as mid-level in the gap will continuously accumulate the excited electronic populations with even faster rate than the valence band(VB) from de-excitation, indicating the energy transfer path has undergone the transient states rather than directly downward de-excitation. To specifically interpret the in-depth influence induced by the surface quencher, we systematically observe the lifetime change of energy levels based on the modulation of the decay rate(K21) and the upconverted energy excitation rate(K1) of surface quencher states in the modelling. With the electron occupation initiated only on the surface quencher and conduction band (CB), the electrons transfer behaviors have been noted with two peaks in distinct decay time, which can be further tuned by the electronic behaviors (K21 and K1) of surface quencher states (**Figure 4d-4e**). Within the increased value of K21/K1, the left-shift of the V_{RE} levels, demonstrating larger separation on the time scale of the two peaks (**Figure 4f** and **Table S5**). This modeling implies the controllability of time-and-spatial entangled luminescence based on the nature of surface defect tuning for prolonging the NEPS effect. Due to the modulations of the electron transfer process between different energy levels are flexible and controllable, it should be also feasible to simulate the electron transfer process in the novel energy storage devices by appropriate coefficient modifications. To evaluate the NPES concept in other electron-related energy transfer system, supplementary calculation results of piezotronic material ZnO also have been added in the ***Supplementary Information.***

Conclusion

In summary, we have established the energy conversion model for the intrinsic nanophotonic energy storage (NPES) effects based on surface defect. With combined DFT calculations and experimental studies above, we realized that the synthesis routes are capable of modifying both the morphology and the overall electronic behaviors. We have proposed the utilization of the LM-SRQT via inhomogeneously distributed surface charge fields to prolong the general charge carrier recombination path. Such charge inhomogeneous distribution on the surface of UCNPs are essentially existed as well as the formation and migration of surface defects states regardless of the stoichiometric ratio. Our previous efforts on NPES effect can be recognized from recent collaborated published work [4]. The discussed surface quantum confinement effect yields from surface vacancy induced Coulomb states (SVIC) states. The following excavation on surface charge density distributions and defect orbitals of surface localized electronics and holes are uncannily parallel with the mechanism in Guerra's work [32]. We outlook beyond the conventional chemical modifications, in the present study, surface electronic processes for efficient NPES can be generally modulated by the LM-SRQT effect. Through this work, we introduced that the non-crystallization of the surface in UCNP dominates the self-activated electronic transitions rather than the size-effect.

Acknowledgement

This work was supported by NSFC (Nos. 21425101, 21321001, 21371011, 21331001) and MOST of China (2014CB643800). The author BH gratefully acknowledges the support of the Natural Science Foundation of China (NSFC) for the Youth Scientist grant (Grant No.: NSFC 11504309, 21771156), the initial start-up grant support from the Department General Research Fund (Dept. GRF) from ABCT in the Hong Kong Polytechnic University (PolyU), and the Early Career Scheme (ECS) fund (Grant No.: PolyU 253026/16P) from the Research Grant Council (RGC) in Hong Kong.

Figure 1.

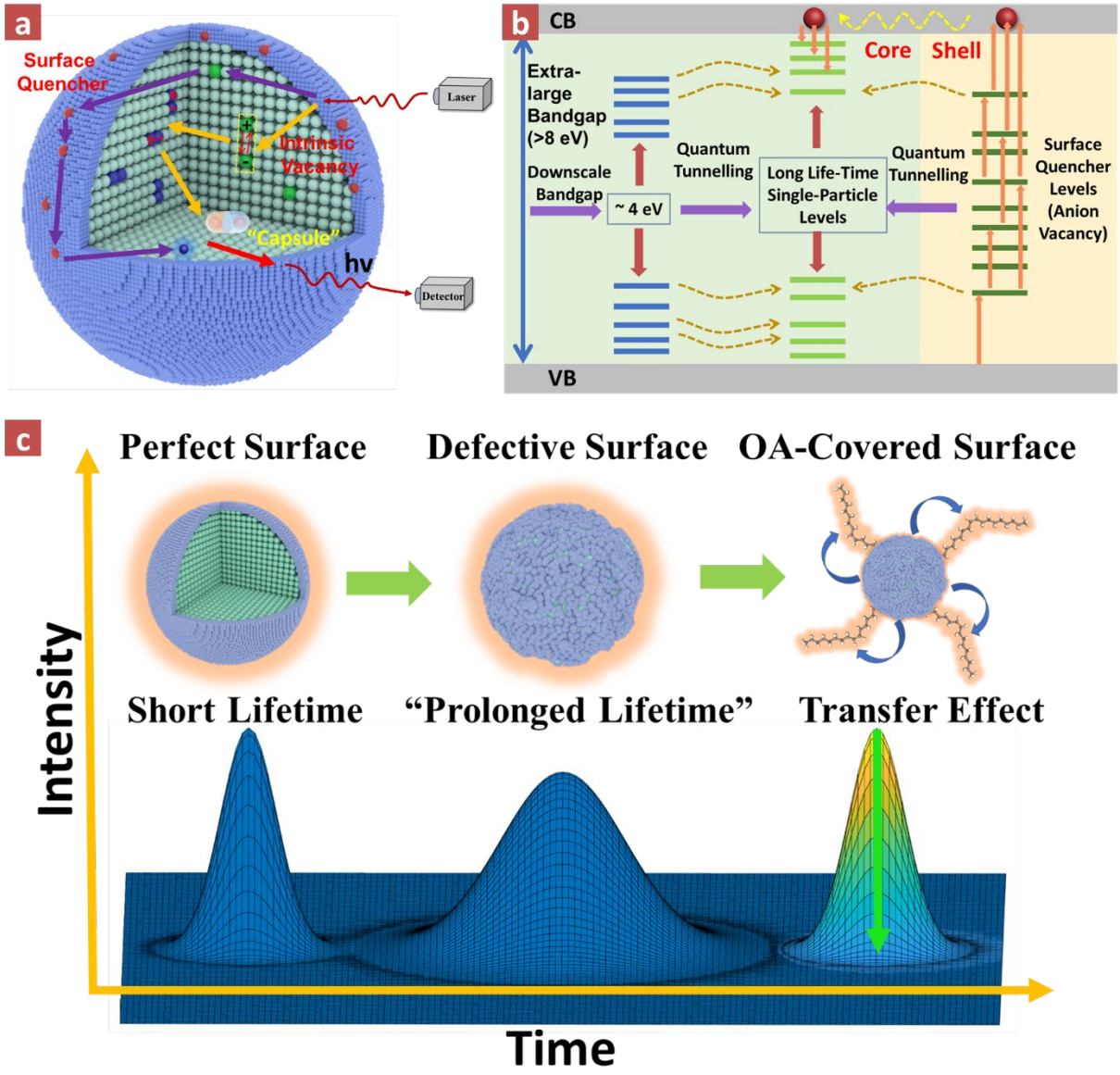

Figure 1. Schematic diagram for the energy transfer mechanism and paths of our proposed NPES concept in $NaREF_4$ (RE=Rare earth ions) nanoparticles. a, Two energy transfer routes are plotted. One for the external excitations to the output centers via the electronically active vacancies and the other is through the surface quencher state on as intermediate state to transfer the excitations to another photo-active site with a prolonged path. **b,** The electron-hole recombination mechanism of the NPES for the UCNPs of $NaREF_4$ with wide optical band gaps. **c,** The generalized diagram of the NPES concept in different nanoparticles.

Figure 2.

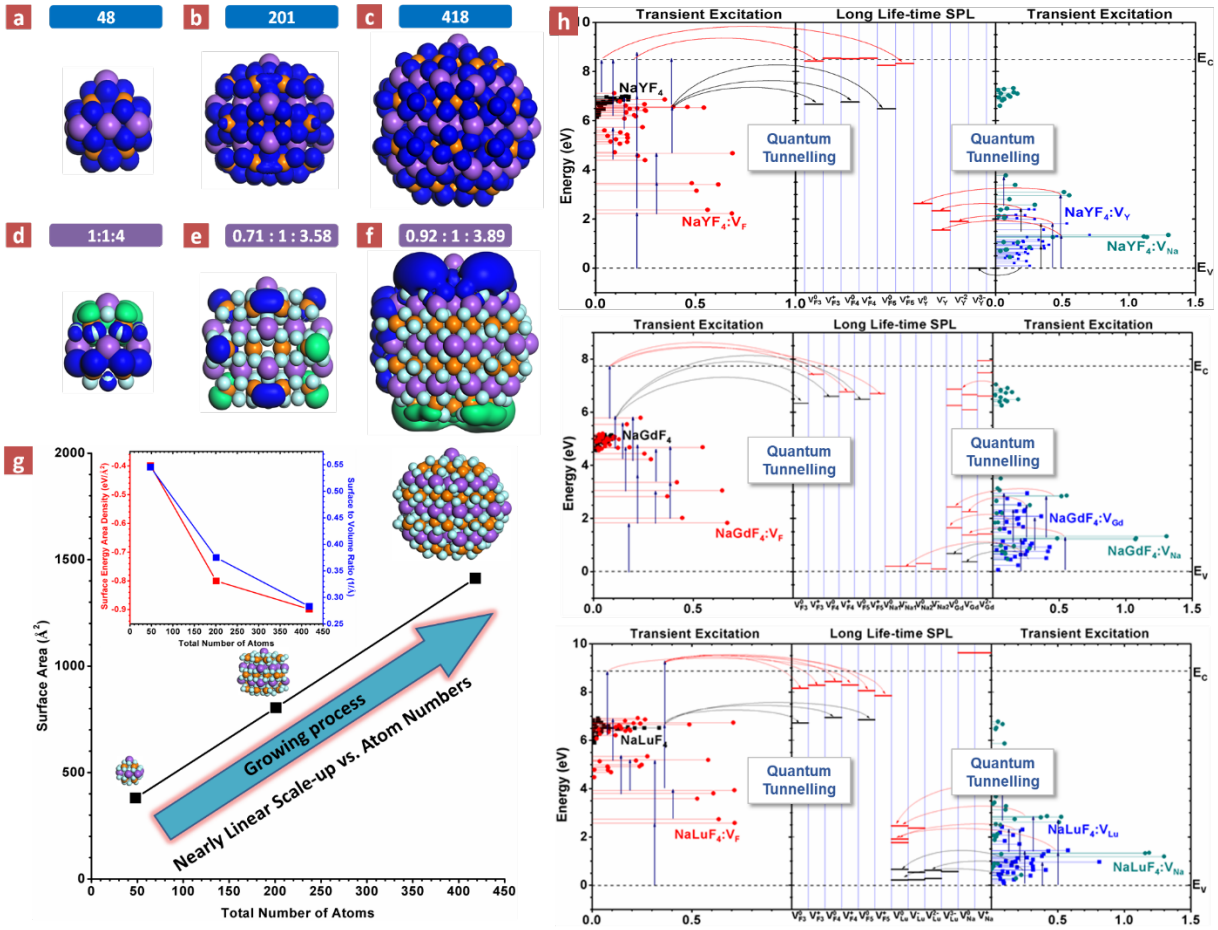

Figure 2. Electronic distribution, particle growth trends, quantum tunnelling effects in energy transfer are shown for $NaYF_4$ UCNPs. a-c, The valence electronic density for different sized $NaYF_4$ nanoparticles, 48-atom, 201-atom, and 418-atom, respectively. **d-f,** Localized electronic and hole orbitals on the surface of the 48-atom, 201-atom, and 418-atom sized $NaYF_4$ respectively (Purple balls = Na, Orange balls = Y, Cyan balls = F; blue isosurfaces=electronic orbitals, green isosurfaces=hole orbitals). **g,** The surface area, surface energy area density σ_s, and surface to volume ratio with related to the size dependence. The number of atoms is the driving variable. **h**, Energy conversion, transfer, and storage via the quantum tunnelling from the transient state excited electrons into the long life-time trapped electrons for $NaREF_4$ (RE=Y, Gd, and Lu).

Figure 3.

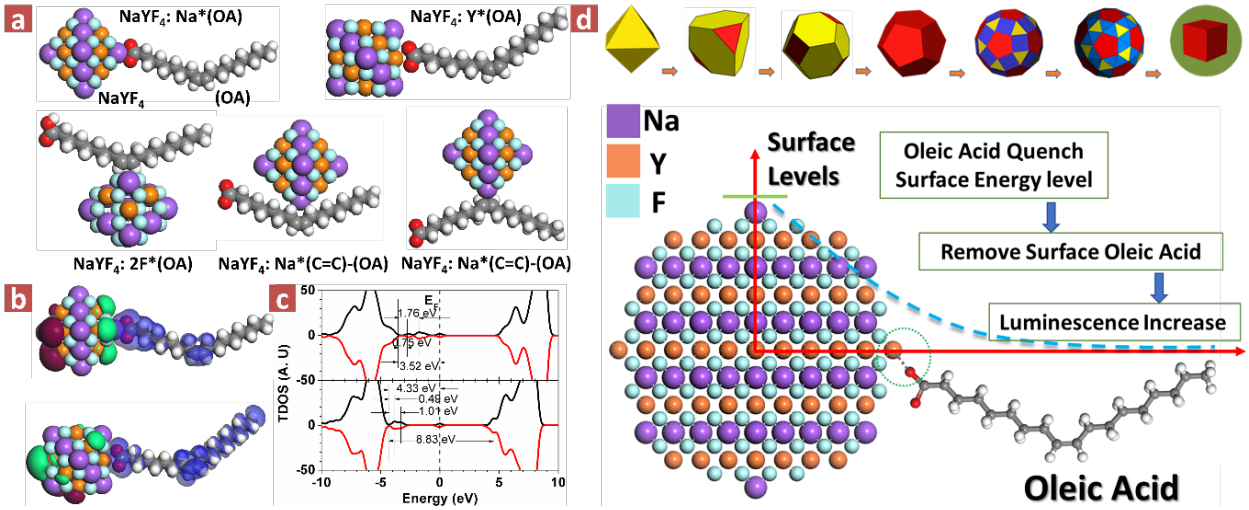

Figure 3. The transfer effect of surface OA ligand on the surface quencher levels. a, site dependence of the oleic acid (OA) molecule locating on the surface of simulated $NaYF_4$ particle model. **b**, The localized electronic orbitals for the oleic ligand adsorbed on the Na and Y sites respectively (blue contour plot=HOMO, green contour plot=LUMO, and the red contour plot=mid-gap localized states). **c**, The total electronic density of states (TDOS) for simulated systems with the oleic ligand adsorbed on the Na and Y sites, respectively. **d, Top**: Schematic diagram for the growth of nanoparticles from octahedron to the final ending as the nearly sphere shaped nanoparticle. The surface effects are originated from the growth process of the nanoparticles. **Bottom:** The illustration of the OA ligand quenching effect on the original surface quencher states of $NaREF_4$ UCNPs, which can prolong energy transfer routes.

Figure 4.

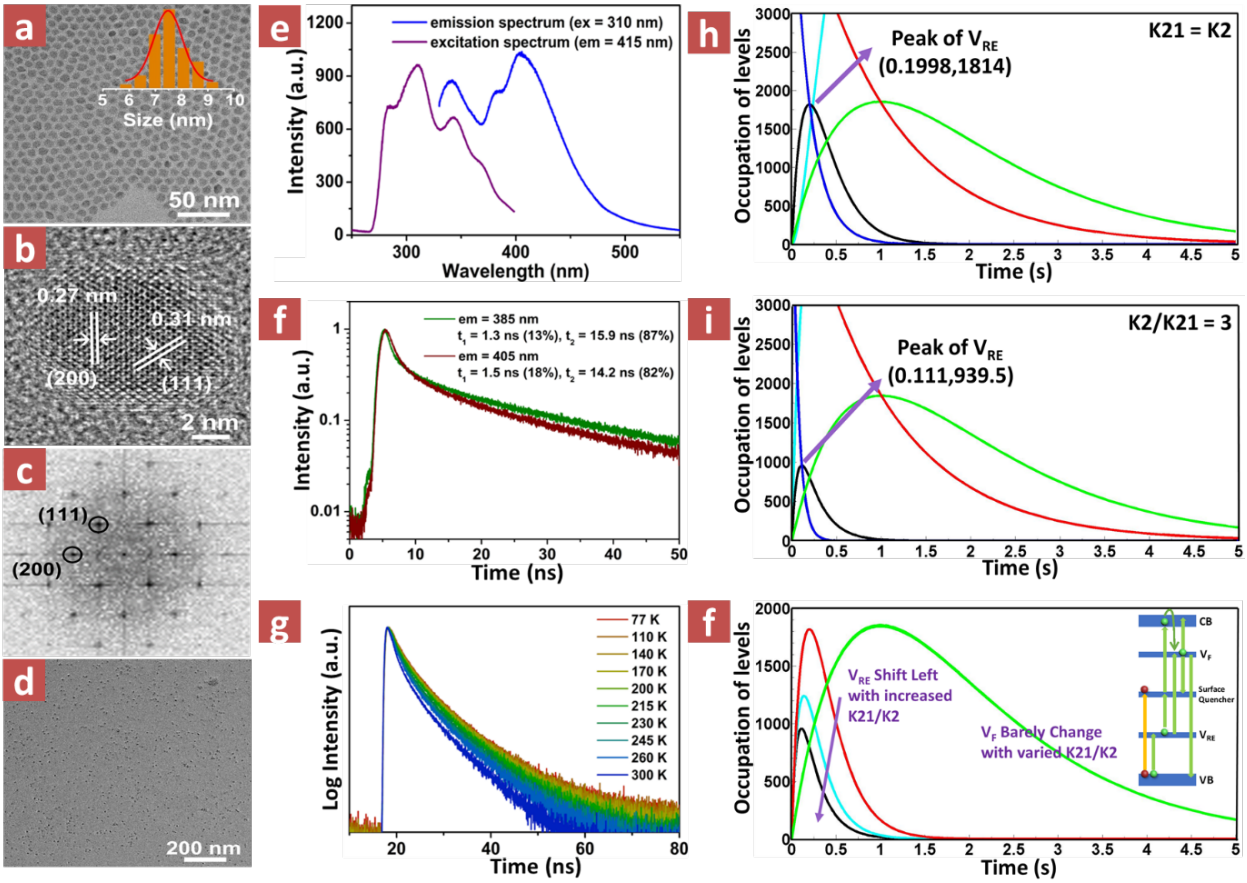

Figure 4. Experimental and mathematical modelling of the dynamic decay behaviors for intrinsic electronic transition of UCNPs. a-c, TEM image, HRTEM image and FFT pattern of as-synthesized $NaYF_4$ nanoparticles. **d,** TEM image of OA-free NaYF4 nanoparticles dispersed in DMF. **e,** Room-temperature fluorescence excitation and emission spectra. **f,** Decay curves of vacancy emissions in $NaYF_4$ nanoparticles dispersed in DMF. The excitation source is a 340 nm pulsed laser. **g,** Temperature-dependent decay curves (λ_{ex} = 340 nm, λ_{em} = 405 nm) of $NaYF_4$ nanoparticles. **h-i,** Mathematical modelling of the five-energy-level system simulated for the $NaREF_4$ nanoparticle with different decay parameters. **f,** The summary of the peak shift of V_{RE} and V_F from the decay parameters change.

References

[1] Z.-S. Wu; G. Zhou; L.-C. Yin; W. Ren; F. Li; H.-M. Cheng, *Nano Energy* **2012,** *1* (1), 107-131.
[2] S. L. Candelaria; Y. Shao; W. Zhou; X. Li; J. Xiao; J.-G. Zhang; Y. Wang; J. Liu; J. Li; G. Cao, *Nano Energy* **2012,** *1* (2), 195-220.
[3] J. Wang; D. Chao; J. Liu; L. Li; L. Lai; J. Lin; Z. Shen, *Nano Energy* **2014,** *7*, 151-160.
[4] Q. Chen; J. Wu; X. Ou; B. Huang; J. Almutlaq; A. A. Zhumekenov; X. Guan; S. Han; L. Liang; Z. Yi; J. Li; X. Xie; Y. Wang; Y. Li; D. Fan; D. B. L. Teh; A. H. All; O. F. Mohammed; O. M. Bakr; T. Wu; M. Bettinelli; H. Yang; W. Huang; X. Liu, *Nature* **2018,** *561* (7721), 88-93.
[5] Z. Pan; Y.-Y. Lu; F. Liu, *Nat Mater* **2012,** *11* (1), 58-63.
[6] T. Aitasalo; P. Dereń; J. Hölsä; H. Jungner; J. C. Krupa; M. Lastusaari; J. Legendziewicz; J. Niittykoski; W. Stręk, *J. Solid State Chem.* **2003,** *171* (1–2), 114-122.
[7] T. Matsuzawa; Y. Aoki; N. Takeuchi; Y. Murayama, *J Electrochem Soc* **1996,** *143* (8), 2670-2673.
[8] F. Liu; W. Yan; Y.-J. Chuang; Z. Zhen; J. Xie; Z. Pan, *Scientific Reports* **2013,** *3*, 1554.
[9] T. Maldiney; A. Bessière; J. Seguin; E. Teston; S. K. Sharma; B. Viana; A. J. J. Bos; P. Dorenbos; M. Bessodes; D. Gourier; D. Scherman; C. Richard, *Nat Mater* **2014,** *13* (4), 418-426.
[10] K. Dong; Z. Wu; J. Deng; A. C. Wang; H. Zou; C. Chen; D. Hu; B. Gu; B. Sun; Z. L. Wang, *Adv Mater* **2018,** *30* (43), e1804944.
[11] Y. Chen; Y. Zhang; Z. Wang; T. Zhan; Y. C. Wang; H. Zou; H. Ren; G. Zhang; C. Zou; Z. L. Wang, *Adv Mater* **2018,** *30* (45), e1803580.
[12] M. Sun; Q. He; X. Kuang; Q. Zhang; S. Ye; B. Huang, *Nano Energy* **2018,** *50*, 88-96.
[13] K. Van den Eeckhout; P. F. Smet; D. Poelman, *Materials* **2010,** *3* (4), 2536.
[14] K. Van den Eeckhout; D. Poelman; P. Smet, *Materials* **2013,** *6* (7), 2789.
[15] P. F. Smet; I. Moreels; Z. Hens; D. Poelman, *Materials* **2010,** *3* (4), 2834.
[16] J. Hölsä, *Electrochem. Soc. Interf.* **2009,** *18*, 42-45.
[17] T. Maldiney; A. Lecointre; B. Viana; A. Bessière; M. Bessodes; D. Gourier; C. Richard; D. Scherman, *J Am Chem Soc* **2011,** *133* (30), 11810-11815.
[18] D. C. Rodríguez Burbano; S. K. Sharma; P. Dorenbos; B. Viana; J. A. Capobianco, *Advanced Optical Materials* **2015,** *3* (4), 551-557.
[19] D. C. Rodriguez Burbano; E. M. Rodriguez; P. Dorenbos; M. Bettinelli; J. A. Capobianco, *Journal of Materials Chemistry C* **2014,** *2* (2), 228-231.
[20] H. Terraschke; C. Wickleder, *Chem. Rev.* **2015**.
[21] R. E. Rojas-Hernandez; F. Rubio-Marcos; R. H. Gonçalves; M. Á. Rodriguez; E. Véron; M. Allix; C. Bessada; J. F. Fernandez, *Inorg. Chem.* **2015,** *54* (20), 9896-9907.
[22] P. Gluchowski; W. Strek; M. Lastusaari; J. Holsa, *Phys. Chem. Chem. Phys.* **2015,** *17* (26), 17246-17252.
[23] M. Allix; S. Chenu; E. Véron; T. Poumeyrol; E. A. Kouadri-Boudjelthia; S. Alahraché; F. Porcher; D. Massiot; F. Fayon, *Chem Mater* **2013,** *25* (9), 1600-1606.
[24] A. Bessière; S. K. Sharma; N. Basavaraju; K. R. Priolkar; L. Binet; B. Viana; A. J. J. Bos; T. Maldiney; C. Richard; D. Scherman; D. Gourier, *Chem. Mater.* **2014,** *26* (3), 1365-1373.
[25] T. Wang; W. Bian; D. Zhou; J. Qiu; X. Yu; X. Xu, *J. Phys. Chem. C* **2015,** *119* (25), 14047-14055.
[26] F. Wang; Y. Han; C. S. Lim; Y. Lu; J. Wang; J. Xu; H. Chen; C. Zhang; M. Hong; X. Liu, *Nature* **2010,** *463* (7284), 1061-1065.

[27] D. Liu; X. Xu; Y. Du; X. Qin; Y. Zhang; C. Ma; S. Wen; W. Ren; E. M. Goldys; J. A. Piper; S. Dou; X. Liu; D. Jin, *Nature Communications* **2016,** *7*, 10254.
[28] F. Wang; X. Liu, *Chem Soc Rev* **2009,** *38* (4), 976-989.
[29] N. Bogdan; F. Vetrone; G. A. Ozin; J. A. Capobianco, *Nano Lett* **2011,** *11* (2), 835-840.
[30] Z. Zhou; W. Zheng; J. Kong; Y. Liu; P. Huang; S. Zhou; Z. Chen; J. Shi; X. Chen, *Nanoscale* **2017,** *9* (20), 6846-6853.
[31] C. Tan; J. Chen; X.-J. Wu; H. Zhang, *Nature Reviews Materials* **2018,** *3*, 17089.
[32] R. E. Guerra; C. P. Kelleher; A. D. Hollingsworth; P. M. Chaikin, *Nature* **2018,** *554*, 346.
[33] S. J. Clark; M. D. Segall; C. J. Pickard; P. J. Hasnip; M. I. J. Probert; K. Refson; M. C. Payne, *Zeitschrift Fur Kristallographie* **2005,** *220* (5/6/2005), 567.
[34] L. Kleinman; D. M. Bylander, *Phys. Rev. Lett.* **1982,** *48* (20), 1425-1428.
[35] S. G. Louie; S. Froyen; M. L. Cohen, *Phys. Rev. B* **1982,** *26* (4), 1738-1742.
[36] I. Grinberg; N. J. Ramer; A. M. Rappe, *Phys. Rev. B* **2000,** *62* (4), 2311-2314.
[37] A. M. Rappe; K. M. Rabe; E. Kaxiras; J. D. Joannopoulos, *Phys. Rev. B* **1990,** *41* (2), 1227-1230.
[38] B. Huang, *J. Comput. Chem.* **2016,** *37* (9), 825-835.
[39] B. Huang, *Solid State Commun* **2016,** *237*, 34-37.
[40] B. Huang, *PCCP* **2016,** *18* (19), 13564-13582.
[41] B. Huang; H. Dong; K.-L. Wong; L.-D. Sun; C.-H. Yan, *J. Phys. Chem. C* **2016,** *120* (33), 18858-18870.
[42] B. Huang, *Phys. Chem. Chem. Phys.* **2017,** *19* (11), 8008-8025.
[43] B. Huang; M. Sun, *Phys. Chem. Chem. Phys.* **2017,** *19* (14), 9457-9469.
[44] B. Huang; M. Sun; D. Peng, *Nano Energy* **2018,** *47*, 150-171.
[45] B. Huang, *Phys. Chem. Chem. Phys.* **2017,** *19* (20), 12683-12711.
[46] Q. Chen; X. Xie; B. Huang; L. Liang; S. Han; Z. Yi; Y. Wang; Y. Li; D. Fan; L. Huang; X. Liu, *Angew Chem Int Ed* **2017,** *56* (26), 7605-7609.
[47] S. Hirata; M. Head-Gordon, *Chem Phys Lett* **1999,** *314* (3–4), 291-299.
[48] H.-X. Mai; Y.-W. Zhang; L.-D. Sun; C.-H. Yan, *The Journal of Physical Chemistry C* **2007,** *111* (37), 13721-13729.
[49] A. Dong; X. Ye; J. Chen; Y. Kang; T. Gordon; J. M. Kikkawa; C. B. Murray, *J Am Chem Soc* **2011,** *133* (4), 998-1006.
[50] L.-D. Sun; Y.-F. Wang; C.-H. Yan, *Accounts. Chem. Res.* **2014,** *47* (4), 1001-1009.
[51] B. Huang; H. Dong; K.-L. Wong; L. Sun; C. Yan, *Journal of Rare Earths* **2017,** *35* (4), 315-334.
[52] B. Huang; M. Sun; A. W. Dougherty; H. Dong; Y.-J. Xu; L.-D. Sun; C.-H. Yan, *Nanoscale* **2017,** *9* (46), 18490-18497.
[53] H. Dong; L.-D. Sun; Y.-F. Wang; J. Ke; R. Si; J.-W. Xiao; G.-M. Lyu; S. Shi; C.-H. Yan, *J Am Chem Soc* **2015,** *137* (20), 6569-6576.
[54] P. Avouris; T. N. Morgan, *The Journal of Chemical Physics* **1981,** *74* (8), 4347-4355.
[55] H.-X. Mai; Y.-W. Zhang; R. Si; Z.-G. Yan; L.-d. Sun; L.-P. You; C.-H. Yan, *J Am Chem Soc* **2006,** *128* (19), 6426-6436.
[56] D. Peng; Q. Ju; X. Chen; R. Ma; B. Chen; G. Bai; J. Hao; X. Qiao; X. Fan; F. Wang, *Chem. Mater.* **2015,** *27* (8), 3115-3120.

TOC

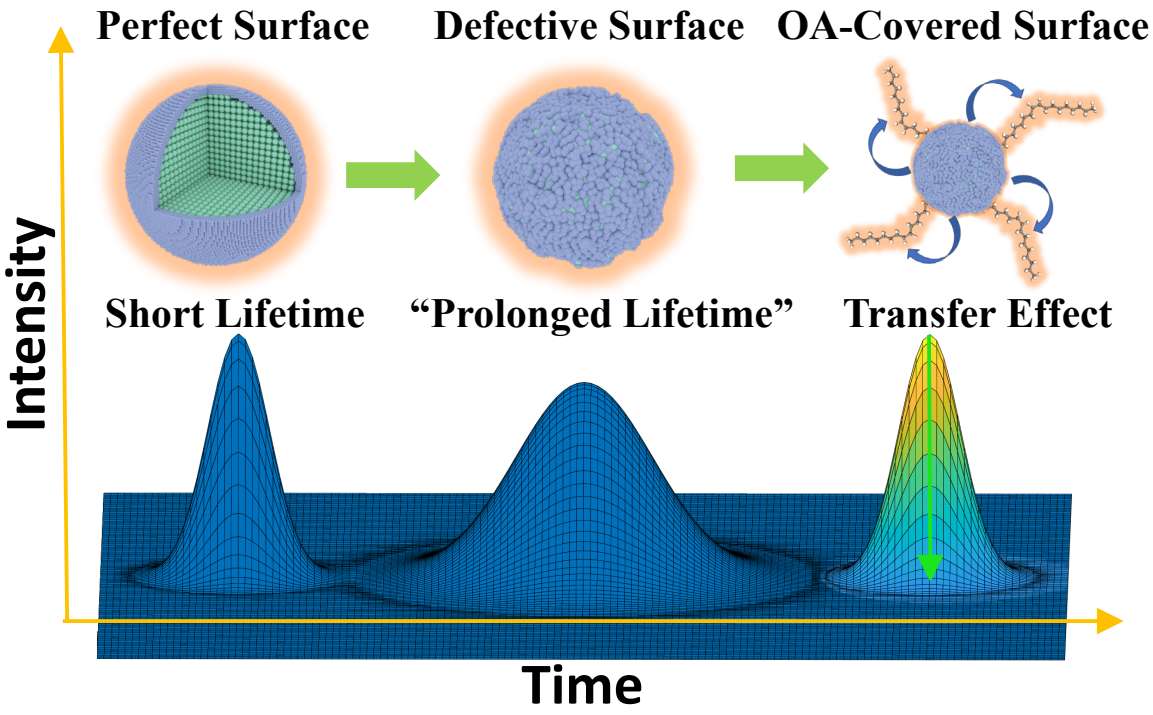

Synopsis

The generalized diagram of the NPES concept is given in different nanoparticles.